Estimation of dynamic friction of the Akatani landslide from seismic waveform inversion and numerical simulation

Masumi Yamada,[1] Anne Mangeney,[2,3] Yuki Matsushi[1] and Laurent Moretti[2,4]

[1]*Disaster Prevention Research Institute, Kyoto University, Uji, Gokasho* 611-0011, *Japan. E-mail:* *masumi@eqh.dpri.kyoto-u.ac.jp*

[2]*Institut de Physique du Globe de Paris, Paris, Sorbonne Paris Cité, Université Paris Diderot, UMR 7154 CNRS, 1 rue Jussieu, F-75005 Paris, France*

[3]*ANGE Team, CEREMA, Inria, Lab. J.-L. Lions, CNRS, 2 rue Simone Iff, F-75012 Paris, France*

[4]*UFR STEP, Université Paris-Diderot 7, 1 rue Jussieu, F-75005 Paris, France*

SUMMARY

We performed numerical simulations of the 2011 deep-seated Akatani landslide in central Japan to understand the dynamic evolution of friction of the landslide. By comparing the forces obtained from numerical simulation to those resolved from seismic waveform inversion, the coefficient of the friction during sliding was investigated in the range of 0.1–0.4. The simulation assuming standard Coulomb friction shows that the forces obtained by the seismic waveform inversion are well explained using a constant friction of $\mu = 0.3$. A small difference between the residuals of Coulomb simulation and a velocity-dependent simulation suggests that the coefficient of friction over the volume is well constrained as 0.3 most of time during sliding. It suggests the sudden loss of shearing resistance at the onset of sliding, that is, sudden drop of the initial coefficient of friction in our model, which accelerates the deep-seated landslide. Our numerical simulation calibrated by seismic data provides the evolution of dynamic friction with a reasonable resolution in time, which is difficult to obtain from a conventional runout simulation, or seismic waveform inversion alone.

Key words: Geomorphology; Friction; Wave propagation.

1 INTRODUCTION

Understanding controlling factors of dynamic friction of catastrophic landslides is an important issue for predicting the velocity and runout distance of a sliding mass, and hence assessing and managing the risks posed by landslides. Several observations based on experimental and field surveys indicate higher mobility in larger landslides (Hsü 1975; Legros 2002; Lucas *et al.* 2014). This implies that as the size of the landslide increases, friction decreases, yet the physical process associated with this empirical relationship remains controversial (Dade & Huppert 1998). For a wet, at least partly saturated landslide body, generation of excess pore pressure by crushing and compaction of basal material may enhance debris mobility, and models incorporating this basal lubrication well explain several cases of long runout landslides (Sassa *et al.* 2010; Wang & Sassa 2010).

In order to clarify the mechanisms of the acceleration of a debris mass, we need to reconstruct the dynamic motion of large bedrock landslides and calculate frictional forces acting on the sliding surface. Previously, landslide motion has been inferred qualitatively from topographic changes caused by the event, and occasionally from eyewitness reports (e.g. Voight & Sousa 1994; Evans *et al.* 2007). However, recent studies show that the use of seismic data may help understand the force history of landslide movement, that

is, the time history of the force acting on the surface and physical parameters (e.g. Kawakatsu 1989; Brodsky *et al.* 2003; Favreau *et al.* 2010; Moretti *et al.* 2012; Allstadt 2013; Ekström & Stark 2013; Yamada *et al.* 2013; Moretti *et al.* 2015). Seismometers are recording continuously with a high sampling rate and sometimes close enough to record signals from smaller landslides. Due to the limited resolution of the data, those previous studies assumed a constant coefficient of friction, however, there was no verification for this assumption.

In this study, we explore the dynamic friction of the 2011 deep-seated Akatani landslide using seismic records and numerical simulation. The event is one of the best recorded catastrophic bedrock landslides with a high-resolution (1 m) digital elevation model (DEM) before and after the landslide and seismic data recorded by bedrock borehole stations with distances from 35 km to over 200 km (Yamada *et al.* 2012; Chigira *et al.* 2013). The accurate DEM of the landslide area enables us to simulate the sliding process by numerical computation, since we have a precise topography and volume of debris. As a result, we can estimate a coefficient of friction and its behaviour during sliding, which enables us to infer physical processes leading to the landslide mass acceleration.

In the past studies, Yamada *et al.* (2013) performed the seismic waveform inversion and obtained the coefficient of friction during sliding, applying the equation of motion for a single point
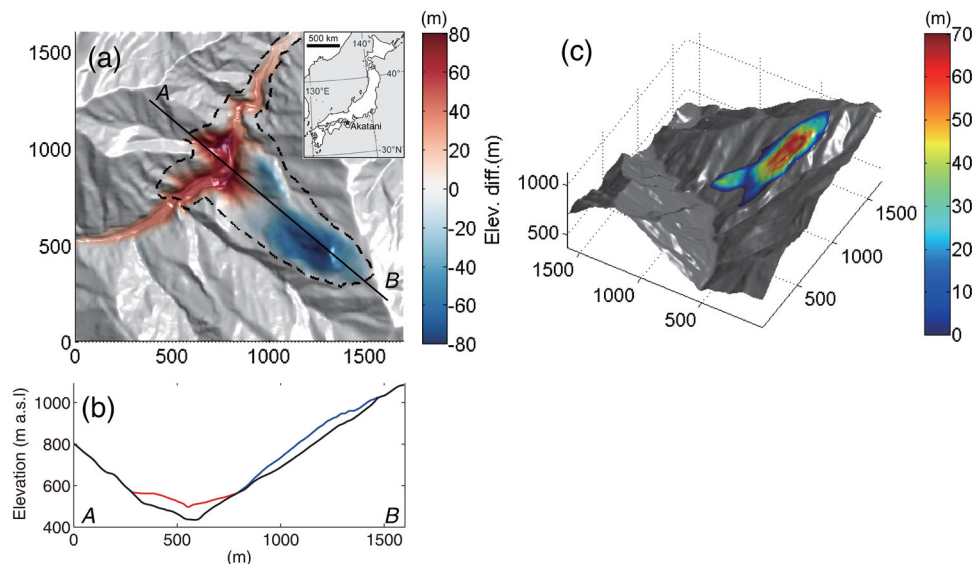
Figure 1. Topography of the Akatani landslide. (a) Elevation changes at the Akatani landslide estimated from airborne LiDAR topographic surveys. Dashed line shows the extent of the landslide. (b) Vertical section along the A–B line (see (a) for location). Red and blue lines show the thickness of the source mass and deposit, respectively. (c) DEM for numerical simulation; colour surface indicates thickness of the mass.

mass. However, the inverted force has limited information at some frequency ranges, since the filtering process is required for the waveform inversion due to heterogeneous velocity structures. With the SHALTOP model for numerical simulation of landslides (Mangeney *et al.* 2007), we were able to obtain the single force from another data set, that is, the DEM. The advantage of this forward calculation is to avoid the loss of information due to the filtering. By comparing this force with that obtained from seismic waveform inversion in the same frequency range, we proposed a friction model, which describes the movements of large bedrock landslides.

2 DATA

On 2011 September 3–4, extensive bedrock landslides occurred across a wide region of the Kii Peninsula as Typhoon Talas produced heavy rainfalls across western Japan (Yamada *et al.* 2012; Chigira *et al.* 2013). The Akatani landslide, one of the largest events, occurred at 16:21:30 on 2011 September 4 (JST) in Nara prefecture, central Japan (135.725°N, 34.126°E). The event consisted of extensive mass movement on a slope approximately 1 km long, inclined at an angle of 30° (Fig. 1). The source volume was 8.2×10^6 m^3 (Yamada *et al.* 2012) and the total mass of displaced material was estimated to be 2.1×10^{10} kg, assuming an average rock density of 2600 kg m^{-3} (Iwaya & Kano 2005).

We obtained a DEM with 1 m grid spacing before and after the landslide from airborne LiDAR data (Yamada *et al.* 2013). The domain of the numerical simulation is 1600 m × 1700 m as shown in Fig. 1(a). Due to the limitation of computation memory, we downsampled the DEM to a 5 m grid. We prepared two topographic data sets from the DEM; the sliding surface and the mass thickness on the surface. The sliding surface was constructed by taking the lower values of the DEMs before and after the landslide. The thickness of the sliding mass was computed by subtracting the DEM for the sliding surface from the DEM before the landslide.

We used three-component forces obtained from a seismic waveform inversion in Fig. 2(a) (Yamada *et al.* 2013). In Yamada *et al.* (2013), the normalized residual of the observed and simulated waveforms is 0.08, which suggests the average error of the amplitude is

about 8 per cent. As we see in the force history in Figs 2(a)–(c), the differences of forces in the numerical simulations for various frictions are more than 8 per cent for the three cases. Therefore, we can determine the coefficient of friction to a resolution of at least 0.1. An acausal fourth-order Butterworth filter with cutoff period of 10 and 100 s was applied to the data to obtain the source-time function. In this relatively long-period window, seismic waveforms are less affected by the heterogeneity in the subsurface structure. For consistency, we apply the same filter to the forces obtained from the numerical simulation, which will be explained in the next section. Note that the horizontal axis of all time-history figures indicates the time after 16:20 (JST), 2011 September 4, in order to be consistent with Yamada *et al.* (2013).

3 METHODS

We used the SHALTOP numerical model to compute the spatiotemporal stress field applied to the sliding surface by the moving landslide mass. This model describes homogeneous, continuous granular flows over 3D topography (Bouchut *et al.* 2003; Bouchut & Westdickenberg 2004; Mangeney-Castelnau *et al.* 2005; Mangeney *et al.* 2007). It is based on the thin-layer approximation and depth-averaging of the Navïer–Stokes equations without viscosity. The flow thickness and depth-averaged velocity in the direction normal to topography are calculated for each grid cell numerically. The topographic data are used for input data, and the friction model can be modulated to control the flow behaviour. The total force acting on the sliding surface can then be computed by summation of the forces applied by the mass at each time step (Moretti *et al.* 2012).

Note that there is an approximation in the model at the onset of simulation. At the time equal to zero, the mass is not in equilibrium, and is released suddenly when the simulation starts. In reality, the initiation of sliding includes the process of fracture, growth of cracks and/or excess pore pressure, which are difficult to include in the current model (George & Iverson 2014; Iverson & George 2014). Therefore, we are not able to distinguish the cohesion and friction at rest in this model. The tangent of the slope angle suggests that the apparent coefficient of friction before the sliding is about 0.6 or
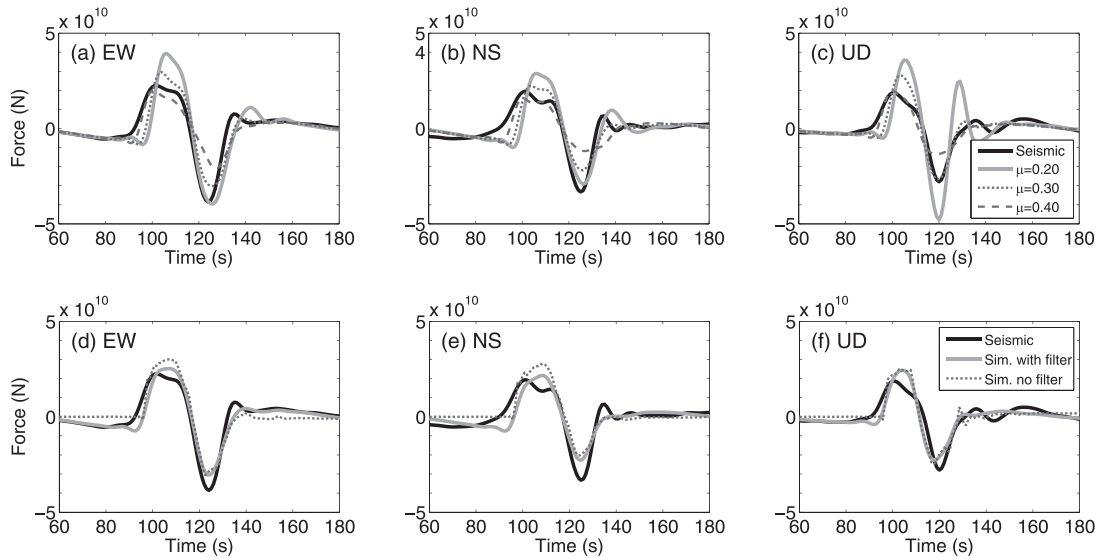
Figure 2. Comparison between the forces obtained from seismic waveform inversion (black lines) and forces obtained from numerical simulations (grey lines). Top (a–c): results assuming constant friction ($\mu = 0.20$, 0.30 and 0.40); waveforms are bandpass filtered between 10 and 100 s. Bottom (d–f): results for the optimal velocity-dependent friction model. Sim. with filter shows the forces bandpass filtered between 10 and 100 s, while sim. no filter shows the forces without filtering. The north–south components ((b) and (e)) are plotted with opposite sign against Yamada *et al.* (2013), so that we can compare the three components easily.

lower (Yamada *et al.* 2013). We use this number as the maximum potential value of the coefficient of friction, since both the cohesive and frictional components contribute to the shearing resistance.

We evaluated different friction models by comparing the simulated force with that obtained from seismic waveform inversion. The normalized residual (hereafter referred to as the residual), defined as the following, is used to evaluate the quality of the fit:

$$R = \frac{\sum_{t=0}^{nt}(f_o(t) - f_s(t - \delta t))^2}{\sum_{t=0}^{nt}(f_o(t))^2} \qquad (1)$$

where $f_o(t)$ and $f_s(t)$ are the force at time t computed from the seismic waveform inversion and numerical simulation, respectively, in 1 s intervals. nt is the total duration of the force. δt is selected to minimize the mean of the residuals for three-component forces.

4 RESULTS

The landslide dynamics are strongly controlled by the flow rheology. Therefore, we can modulate the behaviour of the sliding mass by changing the friction model. In this analysis, we test two different friction laws: Coulomb friction, in which the dynamic coefficient of friction is independent of sliding velocity and a velocity-dependent friction model (Rice 2006; Lucas *et al.* 2014). The resulting forces are compared with those calculated from the seismic waveform inversion by Yamada *et al.* (2013).

4.1 SHALTOP simulation with Coulomb friction

We first test a Coulomb friction model with constant friction coefficient, that is, friction is independent of sliding velocity. We varied the coefficient of friction in several simulations so that the resulting force acting on the sliding surface agrees best with the force obtained from seismic waveform inversion. Figs 2(a)–(c) show the forces obtained by SHALTOP numerical simulation with different coefficients of friction (μ) compared to those from the seismic waveform inversion. Two large pulses at 90–110 and 110–130 s are

well captured by the simulation, but the force amplitudes vary depending on the assumed coefficient of friction. A smaller coefficient of friction causes greater acceleration, and produces a larger peak amplitude of the force. Changing the coefficient of friction controls the amplitude of the forces, but has a smaller effect on the phase of the forces. A larger coefficient of friction better approximates the first peak but the second peak is underestimated. To identify the best-fitting parameter value, we varied the coefficient of friction between 0.2 and 0.4 with an interval of 0.02. The coefficient of friction that minimized the residual is $\mu = 0.30$ and the value of the residual is 0.198.

4.2 SHALTOP simulation with velocity-dependent friction model

Velocity-dependent friction has been observed during earthquakes (e.g. Heaton 1990; Ide & Takeo 1997), landslides (e.g. Yamada *et al.* 2013; Lucas *et al.* 2014) and laboratory rock experiments (e.g. Hirose & Shimamoto 2005; Rice 2006; Han *et al.* 2007). Here, we use the empirical relationship used in Lucas *et al.* (2014):

$$\mu = \frac{\mu_o - \mu_w}{1 + ||U||/U_w} + \mu_w \qquad (2)$$

where μ_o is the static coefficient of friction, μ_w is the dynamic coefficient of friction during sliding and U_w is the characteristic velocity for the onset of weakening. $||U||$ is the vector sum of the velocity at each grid cell. Note that μ_o is the friction coefficient when $||U|| = 0$, μ_w is the coefficient of friction when $||U|| = \infty$ and U_w controls how quickly the coefficient of friction drops as a function of velocity. We computed μ for each grid cell at each time step.

Figs 2(d)–(f) show forces on the sliding surface obtained by numerical simulation using velocity-dependent friction with parameters: $\mu_o = 0.6$, $\mu_w = 0.24$ and $U_w = 4$ m s^{-1}. We selected these parameters, as shown below, by minimizing the residuals of the forces from the seismic waveform inversion and numerical
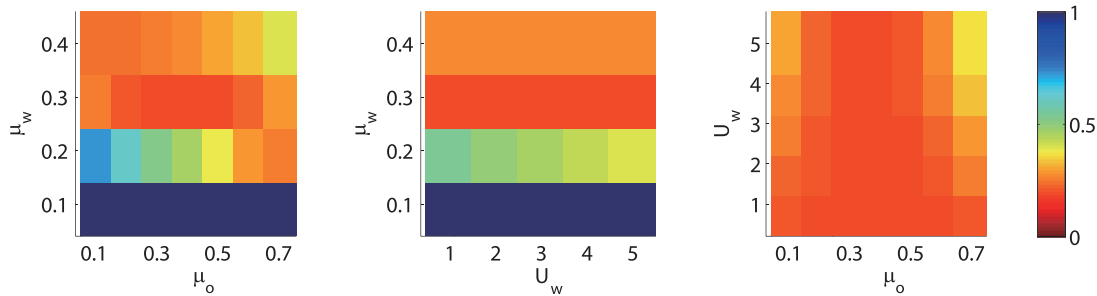
Figure 3. Residual surfaces for pairs of parameters. (a) μ_o versus μ_w, at $U_w = 3$. (b) U_w versus μ_w, at $\mu_o = 0.4$. (c) μ_o versus U_w, at $\mu_w = 0.3$.

simulation. The value of the residual is 0.170, which is slightly lower than the residual of the model assuming Coulomb friction.

4.3 Parameter search for the velocity-dependent friction model

In order to select the optimal parameters for the friction model that best explain the forces obtained through seismic waveform inversion, we performed a 3-D grid search for μ_o, μ_w and U_w in eq. (2). A two-step grid search was performed with the following parameter space: a coarse grid with $\mu_o = (0.1, 0.2, 0.3, 0.4, 0.5, 0.6, 0.7)$, $\mu_w = (0.1, 0.2, 0.3, 0.4)$ and $U_w = (1, 2, 3, 4, 5)$ m s^{-1} and a finer grid over μ_w. The optimal parameter set for the first step is $(\mu_o, \mu_w, U_w) = (0.4, 0.3, 3)$, with a residual of 0.188.

Fig. 3 shows the residual surfaces for a pair of three parameters. The third parameter, which is not shown on each plot, is fixed at the optimum value. For example, in Fig. 3(a), the residual for μ_o and μ_w are plotted, while U_w is fixed at 3.0 m s^{-1}. The plots show that the sensitivity to the parameter μ_w is very high, as the surfaces vary strongly in the vertical direction in Figs 3(a) and (b). The sensitivities to μ_o and U_w are relatively low, as shown in Figs 3(a) and (b), where the peak along that axis is not strong.

Next, we performed a grid search with a smaller interval for the most sensitive parameter μ_w (0.02) between 0.20 and 0.34 around the optimal value of the first step. We obtained the optimal parameter values $(\mu_o, \mu_w, U_w) = (0.6, 0.24, 4)$ with a slightly smaller residual of 0.170. Fig. 4(a) shows the 3D residual space for the parameters. We can see that there is a trade-off among parameters around the most optimal model. In order to evaluate the temporal change of the coefficient of friction, the mass-weighted average of the coefficient of friction for each model in Fig. 4(a) is shown in Fig. 4(b). For

the presentation purpose, the models with μ_o greater than or equal to 0.4 are shown in the figure. Although the velocity of the centre of mass changes significantly in time, the average coefficient of friction is about constant (0.3) between 105 and 130 s. The models with smaller residuals also show that the variation of the coefficient of friction is very small during this period. Therefore, the coefficient of friction is well constrained at around 0.3. However, because of the small amplitude of the force, there is no resolution of the coefficient of friction at the beginning of the simulation and time after 140 s.

4.4 Snapshots of the landslide movement

Yamada *et al.* (2013) interpreted the forces obtained from seismic waveform inversion as being representative of three stages in the landslide process (90–110 s, 110–130 s and 130–140 s in Fig. 2). During the first stage, the mass begins moving and accelerates down the slope. In the second stage, the toe reaches the opposite valley-side slope and the mass starts decelerating. In the third stage, the mass runs slightly backup on the sliding surface and the movement terminates with some continued deformation.

The behaviour of the sliding mass in the SHALTOP numerical simulation is consistent with this interpretation. The first stage corresponds to the first six panels in Fig. 5. Note that the onset of the numerical simulation is 98 s after the reference time (16:20), which might be smeared in the waveform inversion due to the acausal bandpass filtering. In the second stage, which corresponds to the next two panels, the sliding mass reaches the bottom of the valley and starts depositing, but a substantial portion is still sliding down the slope. At 40 s after initiation, movement of the main body is almost over. Since the numerical simulation does not require the bandpass filter, the evolution of the force tends to be sharper, and as
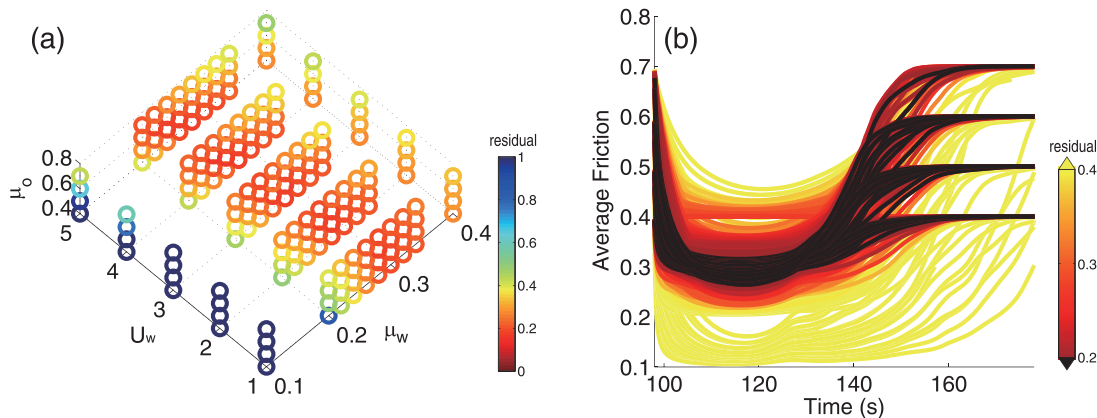
Figure 4. (a) 3-D residual space for a finer grid search. (b) The time history of the average coefficient of friction for each model in (a). Colours indicate the residual of each model. Models with residuals smaller than 0.2 are shown as black lines.
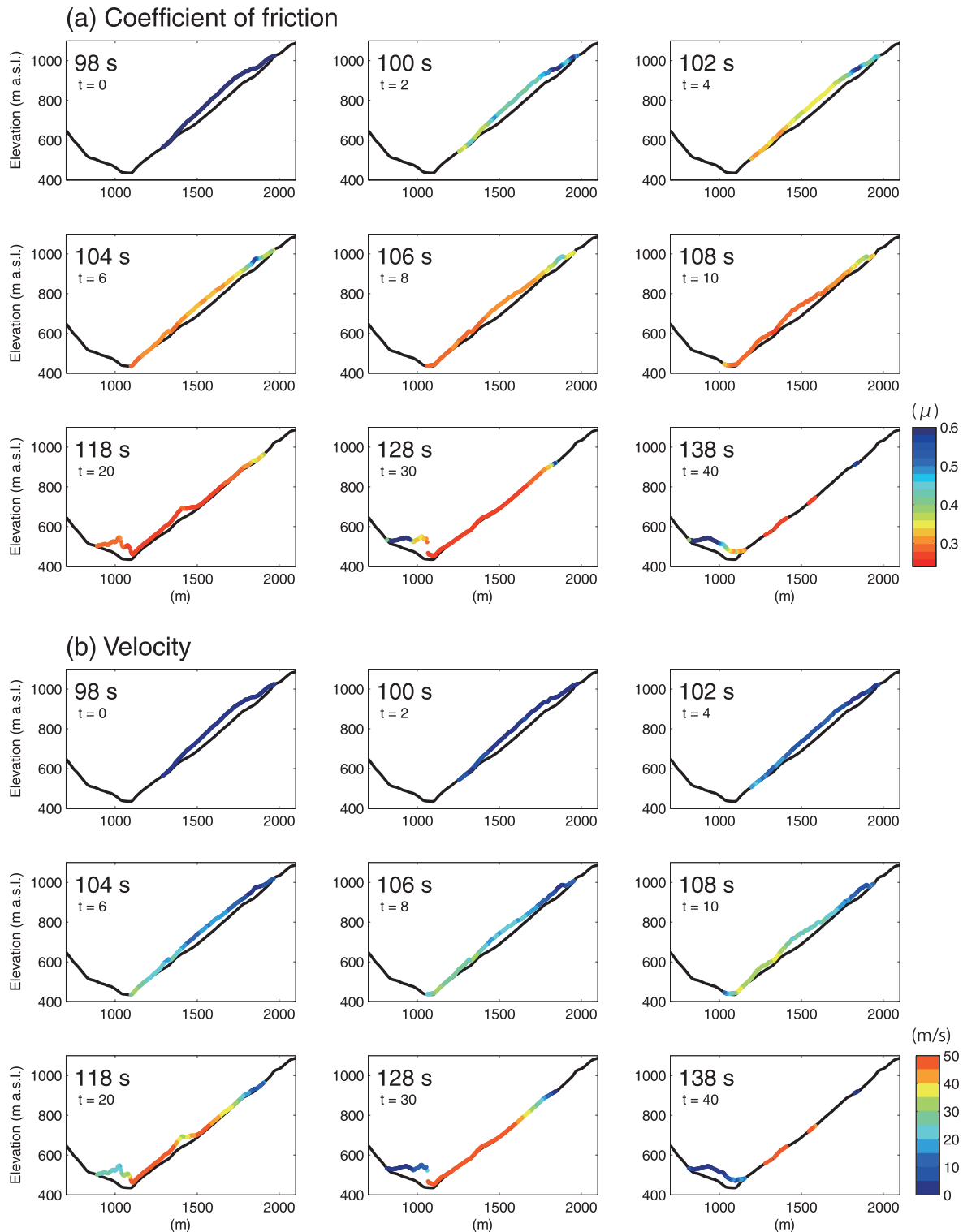
Figure 5. Snapshots of the numerical simulation employing velocity-dependent friction along the section A–B in Fig. 1(a). Colours indicate (a) the coefficient of friction and (b) velocity of the mass at the grid, respectively, and the location of each point shows the thickness of the mass. t_0 is the time of simulation.

a result, the duration of the process becomes shorter. The duration of the three stages is better resolved by the numerical simulation which has a higher resolution in time and space.

Coloured points in Fig. 5 indicate snapshots of the coefficient of friction and velocity on each grid cell along the section A–B in Fig. 1(a). Within 8 s after the initiation of sliding, velocity quickly

increases and the coefficient of friction drops to less than 0.32 for most of the profile. During the first stage, the velocity continues to increase but the coefficient of friction remained nearly constant. In the second stage, the tip of the deposit reaches the bottom of the valley and the mass begins decelerating. Inverted forces are not very sensitive to the third stage, where acceleration is small, but
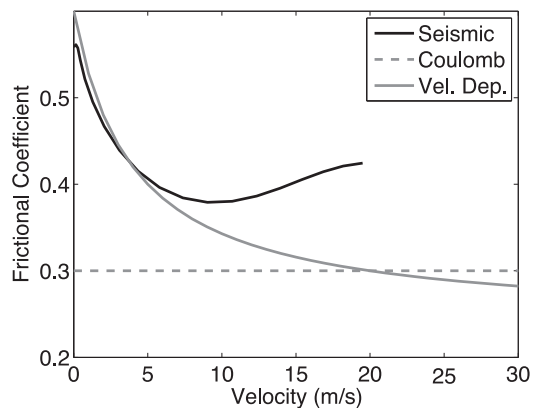
Figure 6. Relationship between velocity and coefficient of friction. Black line shows the result of Yamada *et al.* (2013), dashed and solid grey lines show the optimal values for the Coulomb friction and velocity-dependent friction, respectively.

we resolve a decrease in velocity and an increase of the frictional coefficient.

5 DISCUSSION

The combination of the numerical simulation and seismic waveform inversion helps resolve the time evolution of friction of the Akatani landslide. Our simulation assuming standard Coulomb friction shows that the forces obtained by seismic waveform inversion are well explained using a constant friction of $\mu = 0.3$. When we use a velocity-dependent friction model, although each parameter is not well resolved, the average coefficient of friction during sliding is well constrained at around 0.3. The small difference between the residuals of Coulomb simulation and velocity-dependent simulation suggests that the coefficient of friction is close to 0.3 most of time during sliding. In other words, once the landslide begins sliding, the movement is accelerated rapidly, and the coefficient of friction reaches this steady state. Therefore, increasing the number of parameters in the friction model does not greatly contribute to improve the fit, since the friction reaches a dynamic value very quickly (see Fig. 4b).

The coefficient of friction calibrated by the force of seismic waveform inversion and numerical simulation provides important physical parameters. It suggests that the entire movement can be explained by the dynamic coefficient of friction of 0.3, whereas eq. 1 in Yamada *et al.* (2013) was applicable only for the first stage, and there was no information on the friction in the later part of the movement.

Another advantage of obtaining a coefficient of friction from numerical simulation is to avoid the loss of information due to the filtering in the waveform inversion. Since it is not possible to perform the waveform inversion for the entire frequency band, Yamada *et al.* (2013) used a period range between 10 and 100 s. Therefore, the inverted force includes little information outside of this period range. This bandpass filter removed sharp changes in the waveforms, and tends to suppress maximum amplitudes (see filtered and unfiltered forces in Figs 2(d)–(f)). Since the friction coefficient in Yamada *et al.* (2013) is computed from the force amplitude by using the equation of motion (eq. 1 in Yamada *et al.* 2013), the force may be underestimated, and as a result, the dynamic coefficient of friction was estimated as 0.38, against 0.3 from the numerical simulation (see Fig. 6). The differences of the force amplitudes

between the seismic waveform inversion and numerical simulation, as well as the computation of the volume, are also potential causes of the discrepancy in our respective results. Suppose we substitute the maximum inverted force by the maximum force obtained from the numerical simulation, the coefficient of friction would be estimated as 0.31. Estimating the coefficient of friction from seismic waveform inversion alone has an advantage of simplicity, but we need to pay attention to the overestimation of the dynamic coefficient of friction (e.g. Moretti *et al.* 2015).

In this approach, it is not necessary to use the extent of the final deposit for the validation of the friction models, since the coefficient of friction is calibrated by the force inverted from seismic data. In the later part of the movement, the body of the landslide collapses and it changes into a debris flow. The extent of the deposit (Fig. S1, Supporting Information) may be influenced by the pore pressure change after the collapse in the valley, so it is difficult to constrain the coefficient of friction with the extent.

The coefficient of friction we obtained in this study is consistent with other studies. Lucas *et al.* (2014) proposed an empirical relationship between the effective frictional coefficient and the volume of landslides. The effective frictional coefficient for Akatani landslide is estimated $\mu = 0.29$ based on the relationship. Moretti *et al.* (2015) presented $\mu = 0.33$ for the Mount Meager landslide with the volume in the same order (48.5×10^6 m^3). These results are in a good agreement with our coefficient of friction during sliding.

The force computed from the SHALTOP model shows a rapid increase at the onset of the simulation (see broken lines in Figs 2(d)–(f)). This is because the SHALTOP model has an approximation at the onset of sliding as we mentioned in Section 3. Therefore, the coefficient of friction during the initial few seconds does not have enough accuracy. Since the coefficient of friction is calibrated by the force, there is no resolution of the average coefficient of friction after 140 s in Fig. 4(b), when the amplitude of force is close to zero (see Fig. 2).

Analysis in this study suggests a significant drop in shearing resistance at the onset of rock mass sliding. Assuming that the initial apparent friction is given by the slope angle, the average coefficient of friction for the sliding mass declines rapidly from ∼0.6 to a dynamic coefficient of ∼0.3 within 10 s (see Fig. 4b). This large drop of apparent frictional resistance may be attributed to loss of cohesive strength at subsurface asperities. We assume the sliding surface has a heterogeneous structure, that is, locked sections (asperities) and unlocked sections. A gravity deformation observed in the field over a long precursory timescale (e.g. Chigira *et al.* 2013) is consistent with this assumption of heterogeneous structure. The breakdown of these asperities suddenly reduces the resisting force, and leads to catastrophic movement of the landslide body. The frictional behaviour in this study supports this assumption for the triggering mechanism of catastrophic landslides. The combination of the numerical simulation and seismic waveform inversion leads to a better understanding of the dynamic evolution of friction, however, further studies are needed for landslides of various velocity, size and lithology to examine effects of mass volume and geological structure on the dynamic friction behaviour of the sliding surface.

6 CONCLUSIONS

We performed landslide simulations using the SHALTOP numerical model to explore the dynamics of deep-seated Akatani landslide that occurred at 16:21:30 on 2011 September 4, in central Japan. By combining the numerical simulation and results from a

seismic waveform inversion (Yamada *et al.* 2013), the coefficient of friction during the sliding of the catastrophic landslide was investigated. The simulation assuming standard Coulomb friction shows that the forces obtained by the seismic waveform inversion are well explained using a constant friction of $\mu = 0.3$. A small difference between the residuals of Coulomb simulation and a velocity-dependent simulation suggests that the coefficient of friction is close to 0.3 most of time during sliding. By assuming that the initial friction is given by the slope angle, it suggests the sudden loss of shearing resistance at the onset of sliding, that is, sudden drop of the initial coefficient of friction in our model, which accelerates the deep-seated landslide. Our numerical simulation calibrated by seismic data provides snapshots of the landslide movement and the evolution of dynamic friction, which is difficult to obtain from conventional runout simulations, or seismic waveform inversion alone. The resolution of dynamic friction was reasonably good when the acceleration of a mass movement, that is, the force acting on the sliding surface, was large, but it is difficult to determine the dynamic coefficient of friction at the initiation and end of the movement by this approach. The well-constrained dynamic coefficient of friction obtained from this study will help understand the dynamic mechanics of deep-seated landslides.

ACKNOWLEDGEMENTS

REFERENCES

Allstadt, K., 2013. Extracting source characteristics and dynamics of the August 2010 Mount Meager landslide from broadband seismograms, *J. geophys. Res.,* **118**(3), 1472–1490.

Bouchut, F. & Westdickenberg, M., 2004. Gravity driven shallow water models for arbitrary topography, *Commun. Math. Sci.,* **2**(3), 359–389.

Bouchut, F., Mangeney-Castelnau, A., Perthame, B. & Vilotte, J.-P., 2003. A new model of saint venant and Savage-Hutter type for gravity driven shallow water flows, *C.R. Math.,* **336**(6), 531–536.

Brodsky, E., Gordeev, E. & Kanamori, H., 2003. Landslide basal friction as measured by seismic waves, *Geophys. Res. Lett.,* **30,** 2236, doi:10.1029/2003GL018485.

Chigira, M., Tsou, C.-Y., Matsushi, Y., Hiraishi, N. & Matsuzawa, M., 2013. Topographic precursors and geological structures of deep-seated catastrophic landslides caused by typhoon talas, *Geomorphology,* **201,** 479–493.

Dade, W.B. & Huppert, H.E., 1998. Long-runout rockfalls, *Geology,* **26**(9), 803–806.

Ekström, G. & Stark, C.P., 2013. Simple scaling of catastrophic landslide dynamics, *Science,* **339**(6126), 1416–1419.

Evans, S., Guthrie, R., Roberts, N. & Bishop, N., 2007. The disastrous 17 February 2006 rockslide-debris avalanche on Leyte Island, Philippines: a catastrophic landslide in tropical mountain terrain, *Nat. Hazards Earth Syst. Sci.,* **7**(1), 89–101.

Favreau, P., Mangeney, A., Lucas, A., Crosta, G. & Bouchut, F., 2010. Numerical modeling of landquakes, *Geophys. Res. Lett,* **37,** L15305, doi:10.1029/2010GL043512.

George, D.L. & Iverson, R.M., 2014. A depth-averaged debris-flow model that includes the effects of evolving dilatancy. II. Numerical predictions and experimental tests, *Proc. R. Soc. A: Math. Phys. Eng. Sci.,* **470,** 20130820, doi:10.1098/rspa.2013.0820.

Han, R., Shimamoto, T., Hirose, T., Ree, J. & Ando, J., 2007. Ultralow friction of carbonate faults caused by thermal decomposition, *Science,* **316**(5826), 878–881.

Heaton, T., 1990. Evidence for and implications of self-healing pulses of slip in earthquake rupture, *Phys. Earth planet. Inter.,* **64**(1), 1–20.

Hirose, T. & Shimamoto, T., 2005. Growth of molten zone as a mechanism of slip weakening of simulated faults in gabbro during frictional melting, *J. geophys. Res.,* **110,** B05202, doi:10.1029/2004JB003207.

Hsü, K.J., 1975. Catastrophic debris streams (sturzstroms) generated by rockfalls, *Bull. geol. Soc. Am.,* **86**(1), 129–140.

Ide, S. & Takeo, M., 1997. Determination of constitutive relations of fault slip based on seismic wave analysis, *J. geophys. Res.,* **102,** 27 379–27 391.

Iverson, R.M. & George, D.L., 2014. A depth-averaged debris-flow model that includes the effects of evolving dilatancy. I. Physical basis, *Proc. R. Soc. Lond. A: Math. Phys. Eng. Sci.,* **470,** 20130819, doi:10.1098/rspa.2013.0819.

Iwaya, T. & Kano, K., 2005. Rock densities for the geologic units in the Japanese islands: an estimate from the database PROCK (Physical Properties of Rocks of Japan), *J. geol. Soc. Jpn.,* **111**(7), 434–437.

Kawakatsu, H., 1989. Centroid single force inversion of seismic waves generated by landslides, *J. geophys. Res.,* **94**(B9), 12 363–12 374.

Legros, F., 2002. The mobility of long-runout landslides, *Eng. Geol.,* **63,** 301–331.

Lucas, A., Mangeney, A. & Ampuero, J.P., 2014. Frictional velocity-weakening in landslides on earth and on other planetary bodies, *Nat. Commun.,* **5,** 3417, doi:10.1038/ncomms4417.

Mangeney, A., Bouchut, F., Thomas, N., Vilotte, J. & Bristeau, M., 2007. Numerical modeling of self-channeling granular flows and of their levee-channel deposits, *J. geophys. Res.,* **112,** F02017, doi:10.1029/2006JF000469.

Mangeney-Castelnau, A., Bouchut, F., Vilotte, J., Lajeunesse, E., Aubertin, A. & Pirulli, M., 2005. On the use of Saint Venant equations to simulate the spreading of a granular mass, *J. geophys. Res.,* **110,** B09103, doi:10.1029/2004JB003161.

Moretti, L., Allstadt, K., Mangeney, A., Capdeville, Y., Stutzmann, E. & Bouchut, F., 2015. Numerical modeling of the Mount Meager landslide constrained by its force history derived from seismic data, *J. geophys. Res.,* **120**(4), 2579–2599.

Moretti, L., Mangeney, A., Capdeville, Y., Stutzmann, E., Huggel, C. Schneider D. & Bouchut, F., 2012. Numerical modeling of the mount steller landslide flow history and of the generated long period seismic waves, *Geophys. Res. Lett.,* **39,** L16402, doi:10.1029/2012GL052511.

Rice, J., 2006. Heating and weakening of faults during earthquake slip, *J. geophys. Res.,* **111**(B5), doi:10.1029/2005JB004006.

Sassa, K., Nagai, O., Solidum, R., Yamazaki, Y. & Ohta, H., 2010. An integrated model simulating the initiation and motion of earthquake and rain induced rapid landslides and its application to the 2006 leyte landslide, *Landslides,* **7**(3), 219–236.

Voight, B. & Sousa, J., 1994. Lessons from Ontake-san: a comparative analysis of debris avalanche dynamics, *Eng. Geol.,* **38**(3), 261–297.

Wang, F. & Sassa, K., 2010. Landslide simulation by a geotechnical model combined with a model for apparent friction change, *Phys. Chem. Earth, A/B/C,* **35**(3), 149–161.

Wessel, P. & Smith, W., 1991. Free software helps map and display data, *EOS, Trans. Am. geophys. Un.,* **72**(441), 445–446.

Yamada, M., Matsushi, Y., Chigira, M. & Mori, J., 2012. Seismic recordings of landslides caused by typhoon Talas (2011), Japan, *Geophys. Res. Lett.,* **39,** L13301, doi:10.1029/2012GL052174.

Yamada, M., Kumagai, H., Matsushi, Y. & Matsuzawa, T., 2013. Dynamic landslide processes revealed by broadband seismic records, *Geophys. Res. Lett.,* **40,** 2998–3002.

SUPPORTING INFORMATION

Additional Supporting Information may be found in the online version of this paper:

Movie S1. The snapshots of the height of the mass of each grid for the numerical simulation of the Akatani landslide with velocity dependent friction law.

Movie S2. The snapshots of the coefficient of friction of the mass of each grid for the numerical simulation of the Akatani landslide with velocity dependent friction law.

Figure S1. Total extents of the deposit for (a) observation and (b) numerical simulation. Colours indicate the height of deposit. (http://gji.oxfordjournals.org/lookup/suppl/doi:10.1093/gji/ggw216/-/DC1).

Please note: Oxford University Press is not responsible for the content or functionality of any supporting materials supplied by the authors. Any queries (other than missing material) should be directed to the corresponding author for the paper.